

Chemically resolved scanning tunneling microscopy imaging of Al on p -type $\text{Al}_{0.1}\text{Ga}_{0.9}\text{As}(001)\text{-}c(2\times 8)/(2\times 4)$

M. J. Hale, D. L. Winn, T. J. Grassman, and A. C. Kummel

Department of Chemistry, 0358, University of California, San Diego, La Jolla, California 92093

R. Droopad

Physical Sciences Research Laboratories-Motorola Labs, Tempe, Arizona 85284

(Received 26 May 2004; accepted 16 November 2004; published online 28 March 2005)

The ability to chemically differentiate individual subsurface Al and Ga atoms, when imaging the $\text{Al}_{0.1}\text{Ga}_{0.9}\text{As}(001)\text{-}c(2\times 8)/(2\times 4)$ surface with scanning tunneling microscopy (STM), has been observed for the first time. In filled-state STM images first layer As atoms bonded to second layer Al atoms appear brighter than those bonded to second layer Ga atoms. This effect is only observed experimentally with p -type $\text{Al}_{0.1}\text{Ga}_{0.9}\text{As}$ grown on p -type GaAs substrates and has been computationally modeled with density functional theory (DFT) calculations. It is hypothesized that chemical specificity is not observed on n -type material because the extra surface charge given to first layer As atoms by second layer Al atoms adds negligibly to the filled-state density of the surface, thus preventing the visualization of chemical specificity with filled-state STM imaging. The ability to distinguish whether first layer As atoms are bonded to second layer Ga and/or Al atoms in STM images shows that small differences in bond ionicity affect the local electronic structure of the material. © 2005 American Institute of Physics. [DOI: 10.1063/1.1846051]

I. INTRODUCTION

Development of a GaAs-based metal-oxide-semiconductor field effect transistor (MOSFET) has been sought after for more than four decades.^{1–10} A GaAs-based MOSFET potentially offers better power added efficiency than current GaAs heterojunction bipolar transistors (HBTs) and greater power density than current GaAs pseudomorphic high electron mobility transistors (PHEMPT). Immediately, a GaAs-based MOSFET could be used to reduce power consumption in base stations until GaN technology can be fully realized.

Commercially available AlGaAs/GaAs interfaces can be found in several different devices,^{11–16} and numerous cross-sectional studies have been performed to characterize the interface.^{17–22} Although the cross section of AlGaAs has been rigorously studied with scanning tunneling microscopy (STM), the (001) surface has yet to be fully characterized.^{18,22,23} As new innovative devices are fabricated, an understanding of the AlGaAs(001) surface will become imperative for optimal device performance.

In this paper, we will show the first atomically, and even more important, chemically resolved images of the $\text{Al}_{0.1}\text{Ga}_{0.9}\text{As}(001)\text{-}c(2\times 8)/(2\times 4)$ surface. Through filled-state STM imaging, it is found that second layer Al atoms cause adjacent first layer As atoms to image 0.1–0.4 Å higher than As atoms bonded to second layer Ga atoms. The ability to determine the atomic location of second layer Al atoms by visualizing slight changes in bond ionicity was only found on p -type material. It is hypothesized that chemical specificity is not observed in n -type material because the extra surface charge donated from second layer Al atoms add negligibly to the n -type character of the filled-state density of the surface As atoms.

II. EXPERIMENTAL TECHNIQUE

Experiments were performed using an ultrahigh vacuum (UHV) chamber equipped with low energy electron diffraction (LEED), Auger electron spectroscopy (AES), mass spectrometry, and a Park Scientific STM. All p - and n -type $\text{Al}_{0.1}\text{Ga}_{0.9}\text{As}(001)$ and GaAs (001) samples were grown by molecular beam epitaxy (MBE) and doped with $2 \times 10^{18} \text{ cm}^{-3}$ Zn and $2 \times 10^{18} \text{ cm}^{-3}$ Si, respectively. A 60 nm As-cap was deposited on each surface to prevent contamination when transferring the samples in atmospheric pressure from the MBE chamber to the experimental STM chamber. Once transferred to the STM chamber, the clean $c(2 \times 8)/(2 \times 4)$ surfaces are obtained by thermally desorbing the protective As-cap. This procedure has been optimized and has been proven to be a successful technique for acquiring clean GaAs(001)- $c(2 \times 8)/(2 \times 4)$ surfaces.^{24,25} The LEED pattern of the decapped samples were sharp; consistent with the well-ordered $c(2 \times 8)/(2 \times 4)$ surfaces observed with STM.

III. EXPERIMENTAL RESULTS

Figures 1(a) and 1(b) show filled-state STM images of p -type $\text{Al}_{0.1}\text{Ga}_{0.9}\text{As}(001)\text{-}c(2 \times 8)/(2 \times 4)$ and GaAs(001)- $c(2 \times 8)/(2 \times 4)$ surfaces, respectively. From these large-scale images the two surfaces appear indistinguishable. Both images show bright As dimer pair rows separated by dark troughs that run in the $[\bar{1}10]$ direction. The troughs contain third layer As dimers which lie 2 Å below the As dimer pairs rows. Each large-scale image shows three separate terraces which have 2 Å step heights. When scanning, a constant current tunneling mode was utilized to allow the tip to adjust to the contours of the surface. By

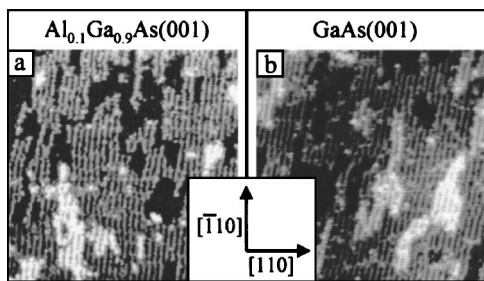


FIG. 1. $650 \times 650 \text{ \AA}$ filled-state ($V = -3 \text{ V}$, $I_T = 0.2 \text{ nA}$) STM images of clean *p*-type (a) $\text{Al}_{0.1}\text{Ga}_{0.9}\text{As}(001)\text{-}c(2 \times 8)/(2 \times 4)$ and (b) $\text{GaAs}(001)\text{-}c(2 \times 8)/(2 \times 4)$. At this scan size, the two surfaces are indistinguishable.

having an active feedback loop, the tip is able avoiding crashing into both the troughs and steps. Both images in Fig. 1 were taken with an applied bias of -3 V and a tunneling current of 0.2 nA . Empty-state (positive bias) imaging was attempted on the $\text{Al}_{0.1}\text{Ga}_{0.9}\text{As}(001)\text{-}c(2 \times 8)/(2 \times 4)$ surface, but similar to $\text{GaAs}(001)\text{-}c(2 \times 8)/(2 \times 4)$,²⁶ only poor resolution was obtained.

A high resolution scan of each surface is pictured in Fig. 2. The high resolution scans show a clear difference between the $\text{Al}_{0.1}\text{Ga}_{0.9}\text{As}(001)\text{-}c(2 \times 8)/(2 \times 4)$ and $\text{GaAs}(001)\text{-}c(2 \times 8)/(2 \times 4)$ surfaces. As seen in Fig. 2(a), some of the As atoms on the As dimer row of the clean $\text{Al}_{0.1}\text{Ga}_{0.9}\text{As}(001)\text{-}c(2 \times 8)/(2 \times 4)$ surface appear brighter than others. This is in contrast to the image of the clean $\text{GaAs}(001)\text{-}c(2 \times 8)/(2 \times 4)$ surface seen in Fig. 2(c), where the As dimer row has a uniform brightness. The atomic position of each atom in Fig. 2(a) was determined by detailed line scan analysis, and is shown in a ball-and-stick diagram in Fig. 2(b).

The enhanced brightness of some of the As atoms on the $\text{Al}_{0.1}\text{Ga}_{0.9}\text{As}(001)\text{-}c(2 \times 8)/(2 \times 4)$ surface, Figs. 3(a)–3(c), indicates a higher filled-state electron density in these atoms than the “typical” surface As atom bonded to two second layer Ga atoms (GaAs_{Ga}). The enhanced brightness is due to second layer Al atoms donating more charge to first layer As atoms than second layer Ga atoms (i.e., greater bond ionicity). The Al atom is less electronegative and has lower ionization energy than Ga which results in the AlAs_{Al} and AlAs_{Ga}

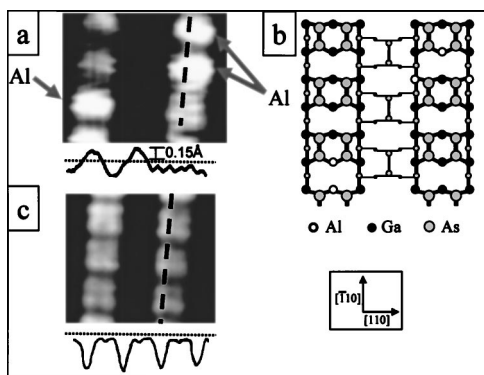


FIG. 2. High resolution images of *p*-type (a) $\text{Al}_{0.1}\text{Ga}_{0.9}\text{As}(001)\text{-}c(2 \times 8)/(2 \times 4)$ and (c) $\text{GaAs}(001)\text{-}c(2 \times 8)/(2 \times 4)$ surfaces. Both images contain a line scan which shows that second layer Al atoms inducing a greater electron density on surface As atoms causing them to image $0.1\text{--}0.2 \text{ \AA}$ above As atoms bonded to second layer Ga atoms. The corresponding ball-and-stick diagram for part (a) is seen in (b).

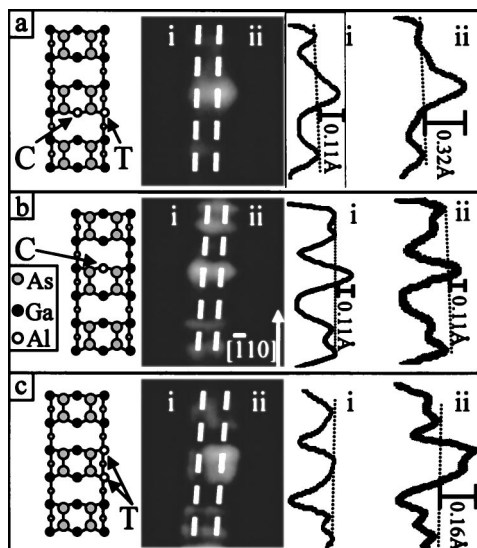


FIG. 3. STM images ($V = -3 \text{ V}$, $I_T = 0.2 \text{ nA}$) of regions of *p*-type $\text{Al}_{0.1}\text{Ga}_{0.9}\text{As}(001)\text{-}c(2 \times 8)/(2 \times 4)$ that contain second layer Al atom(s) and their corresponding ball-and-stick diagrams and line scans. Center Al atoms are labeled “C” and trough Al atoms are labeled “T.” Part (a) shows a center and trough Al atom bonded to the same surface As atom. Part (b) shows a center Al atom. Part (c) shows trough Al atoms.

atoms being more electron rich than the GaAs_{Ga} atoms. The observed result in STM is a $0.1\text{--}0.4 \text{ \AA}$ measured height increase in AlAs_{Ga} atoms and AlAs_{Al} atoms compared to GaAs_{Ga} atoms. The observed height increase depends on the position and number of the second layer Al atoms as well as the tip morphology.

Figure 3 shows three different second layer Al bonding configurations and their corresponding line scans. The imaged sites are all taken from the same large-scale STM image in order to maintain constant tip morphology and achieve an accurate comparison between each site. The largest measured height increase results from AlAs_{Al} sites, as in Fig. 3(a). The observed height increase for the AlAs_{Al} site is 0.32 \AA , as measured from line scan “ii.” The second As atom bonded to a single Al atom (GaAs_{Al}) in Fig. 3(a) only shows an observed height increase of 0.11 \AA , as measured from line scan “i.” The excess charge donated by the center Al atom, labeled “C,” is divided between two surface As atoms, whereas the trough Al atom, labeled “T,” donates its excess charge to only one surface As atom. Therefore, the As atom bonded to two different second layer Al atoms appears nearly three times higher than the As atom next to it bonded to a single second layer center Al atom.

Figure 3(b) shows another example of a second layer center Al atom, also labeled “C.” Unlike the center Al atom seen in Fig. 3(a), Fig. 3(b) shows the effect of an isolated center Al atom. Line scans “i” and “ii” taken along the As dimer row in Fig. 3(b), show that the center Al atom donates its charge symmetrically to the two surface As atoms that it is bonded with. The measured height increase for both As atoms in line scans “i” and “ii” is 0.11 \AA , the same as line scan “i” in Fig. 3(a).

Figure 3(c) shows two separate sites in which an As atom is bonded to one center Ga atom and one Al atom occupying the trough site. Line scan “i” from Fig. 3(c) shows

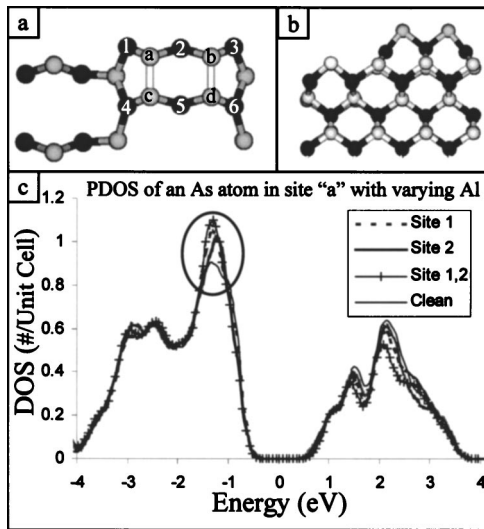


FIG. 4. Part (a) shows a top down cut-away view of the (2×4) slab with the possible location of second layer Al atoms labeled 1–6, and first layer As atoms labeled a–d. Part (b) shows a side view of the 8 layer slab. Part (c) shows the PDOS of an As atom in position “a” from a clean slab and with second layer Al occupying site (1), (2), and (1 and 2). Where the position of the As atom and second layer Al is defined in (a).

that the Al atoms have no effect on the observed height of neighboring As atoms (As atoms bonded to the same center Ga atom). However, a measured height increase of 0.16 \AA is observed for both As atoms bonded directly to the trough Al atoms as seen in line scan “ii” in Fig. 3(c).

Although excess charge on the surface induced by second layer Al atoms is readily observed in *p*-type Al_{0.1}Ga_{0.9}As(001)-*c*(2×8)/(2×4) STM images, the effect is not observed with *n*-type Al_{0.1}Ga_{0.9}As(001)-*c*(2×8)/(2×4). It is hypothesized that the excess surface charge donated from second layer Al atoms is overshadowed by the already electron rich *n*-type character of the bulk, which prevents the visualization of the small effect of extra charge transfer by Al in filled-state STM imaging.

IV. COMPUTATIONAL RESULTS

We have performed density functional theory (DFT) calculations to confirm our experimental findings. The calculations were performed with the Vienna *Ab-Initio* Simulation Package (VASP) (Refs. 27–30) using the generalized gradient approximation (GGA, PW91), and ultrasoft Vanderbilt pseudopotentials (as supplied with the VASP program).^{31,32} A $4 \times 2 \times 1$ Monkhorst–Pack *k*-point mesh generation scheme (for a total of 2 irreducible *k*-points) and a plane-wave kinetic energy cut-off of 500 eV was used. A single (2×4) reconstructed unit cell was used, consisting of eight atomic layers with a (001) orientation, and bottom terminated with hydrogen. The top-down view of the first layer as well as a side view of the entire slab can be seen in Figs. 4(a) and 4(b), respectively.

Figure 4(c) shows the partial density of states (PDOS) associated with an As atom in position “a” without second layer Al, and with Al atoms in positions (1), (1 and 2), and (2), where all positions are defined in part (a). From this graph it is easy to see that the PDOS of the surface As atom

increases in the vicinity of -1.5 eV as the second layer Al is added. When the surface filled-state DOS is probed with STM the increase in the DOS originating from $_{\text{Al}}\text{As}_{\text{Ga}}$ [positions (1) and (2)] and $_{\text{Al}}\text{Al}_{\text{Al}}$ atoms [position (1 and 2)] is able to be visualized for *p*-type material.

An increase in the filled-state DOS associated with $_{\text{Al}}\text{As}_{\text{Al}}$ and $_{\text{Al}}\text{As}_{\text{Ga}}$ atoms near -1.5 eV is seen for all other calculated structures. Other calculated structures include Al atoms occupying position (1 and 3), (1 and 4), (1 and 5), and (2 and 5), where the positions of the Al atoms are again referenced to Fig. 4(a). It should also be noted that the Al atom in position 2 had the smallest affect on the DOS of the As atoms bonded directly to the Al atom because the effect is divided between two As atoms, and the greatest increase in the DOS of an As atom came when two Al atoms were bonded to it [position (1 and 2)].

The calculated DOS associated with each surface As atom were integrated over -3 eV to 0 eV , the region probed experimentally with STM. The integrated DOS is used only as a qualitative measure because the exact work function offset between the tip and sample are unknown due to an ever changing tip chemical makeup and morphology.³³ It was found that the calculated DOS from each As atom were in excellent qualitative agreement with our experimental findings. The greatest DOS was found to come from a surface As atom bonded to two second layer Al atoms, followed by an As atom bonded to a second layer tri-coordinated Al atom, and the smallest increase was from an As atom bonded to a single tetrahedrally bonded Al atom.

V. DISCUSSION AND CONCLUSION

In summary, we have shown that second layer Al atoms donate more charge to first layer As atoms than second layer Ga atoms. The extent of charge donation varies, depending upon the number and coordination of second layer Al atom(s) bonded to first layer As atoms. The extra charge on the surface As atoms bonded to Al results in an experimentally observed increase in the surface height when measured with STM. This result can be explained by the lower electronegativity and ionization energy of Al compared to Ga. By taking detailed line scans along experimental STM images, it is possible to chemically resolve the exact atomic position of second layer Al atoms on *p*-doped Al_{0.1}Ga_{0.9}As(001)-*c*(2×8)/(2×4). It is hypothesized that the extra surface charge on surface As atoms bonded to second layer Al atoms adds negligibly to the filled-state density of surface As atoms on *n*-type material, preventing the visualization of chemical specificity.

Our experimental results were confirmed through DFT calculations which showed excellent qualitative agreement between the increased height observed experimentally in STM images and the calculated magnitude of the DOS per As atom. Both experimental height and calculated DOS of individual As atoms varied in the same manner depending on the number and coordination of second layer Al atoms.

The enhanced surface charge, emanating from As atoms bonded to second layer Al atoms, allows the visualization of the difference in bond ionicity between Al bonded to As and

Ga bonded to As. The charge separation, observed in STM, shows that the bond between Al and As is observably more ionic in nature than the bond between Ga and As, even when the Al and Ga atoms are fully embedded (tetrahedrally bonded) within the bulk material.

- ¹N. Yokoyama, T. Mimura, and M. Fukuta, *IEEE Trans. Electron Devices* **27**, 1124 (1980).
- ²B. Bolliger, M. Erbudak, M. Hong, J. Kwo, A. R. Kortan, and J. P. Mannaerts, *Surf. Interface Anal.* **30**, 514 (2000).
- ³A. Colquhoun, E. Kohn, and H. L. Hartnagel, *IEEE Trans. Electron Devices* **25**, 375 (1978).
- ⁴C. J. Huang, Z. S. Ya, J. H. Horng, M. P. Houg, and Y. H. Wang, *Jpn. J. Appl. Phys., Part 1* **41**, 5561 (2002).
- ⁵H. Takagi, G. Kano, and I. Teramoto, *IEEE Trans. Electron Devices* **25**, 551 (1978).
- ⁶E. Kohn and A. Colquhoun, *Electron. Lett.* **13**, 73 (1977).
- ⁷Y. C. Wang, M. Hong, J. M. Kuo, J. P. Mannaerts, J. Kwo, H. S. Tsai, J. J. Krajewski, Y. K. Chen, and A. Y. Cho, *IEEE Electron Device Lett.* **20**, 457 (1999).
- ⁸J. Y. Wu, H. H. Wang, Y. H. Wang, and M. P. Houg, *IEEE Trans. Electron Devices* **48**, 634 (2001).
- ⁹P. D. Ye, G. D. Wilk, B. Yang, J. Kwo, H. J. L. Gossmann, M. Hong, K. K. Ng, and J. Bude, *Appl. Phys. Lett.* **84**, 434 (2004).
- ¹⁰H. Becke, R. Hall, and J. White, *Solid-State Electron.* **8**, 813 (1965).
- ¹¹M. Osinski, V. A. Smagley, M. Lu, G. A. Smolyakov, P. G. Eliseev, B. P. Riely, P. H. Shen, and G. J. Simonis, *IEEE J. Sel. Top. Quantum Electron.* **9**, 1422 (2003).
- ¹²E. A. Camargo, H. M. H. Chong, and R. M. De la Rue, *Opt. Express* **12**, 588 (2004).
- ¹³A. Cavallini, G. Verzellesi, A. F. Basile, C. Canali, A. Castaldini, and E. Zanoni, *J. Appl. Phys.* **94**, 5297 (2003).
- ¹⁴S. Y. Cheng, *Superlattices Microstruct.* **33**, 1 (2003).
- ¹⁵M. Graf, G. Scalari, D. Hofstetter, J. Faist, H. Beere, E. Linfield, D. Ritchie, and G. Davies, *Appl. Phys. Lett.* **84**, 475 (2004).
- ¹⁶S. Hofling, A. Bazhenov, M. Fischer, J. Seufert, A. Wolf, M. Emmerling, J. P. Reithmaier, and A. Forchel, *Electron. Lett.* **40**, 120 (2004).
- ¹⁷M. B. Johnson, M. Pfister, S. F. Alvarado, and H. W. M. Salemink, *Microelectron. Eng.* **27**, 31 (1995).
- ¹⁸S. Kasai, N. Negoro, and H. Hasegawa, *Appl. Surf. Sci.* **175**, 255 (2001).
- ¹⁹H. Salemink and O. Albrektsen, *J. Vac. Sci. Technol. B* **9**, 779 (1991).
- ²⁰M. Manimaran, P. R. Vaya, and T. Kanayama, *J. Lumin.* **87-9**, 1158 (2000).
- ²¹R. F. Kopf, E. F. Schubert, T. D. Harris, R. S. Becker, and G. H. Gilmer, *J. Appl. Phys.* **74**, 6139 (1993).
- ²²T. Takahashi, M. Yoshita, and H. Sakaki, *Appl. Phys. Lett.* **68**, 502 (1996).
- ²³N. Inoue, M. Tanimoto, K. Kanisawa, S. Hirono, J. Osaka, and Y. Homma, *J. Cryst. Growth* **127**, 956 (1993).
- ²⁴M. J. Hale, S. I. Yi, J. Z. Sexton, A. C. Kummel, and M. Passlack, *J. Chem. Phys.* **119**, 6719 (2003).
- ²⁵M. J. Hale, J. Z. Sexton, D. L. Winn, A. C. Kummel, M. Erbudak, and M. Passlack, *J. Chem. Phys.* **120**, 5745 (2004).
- ²⁶M. C. Gallagher, J. Kim, and R. F. Willis, *J. Vac. Sci. Technol. A* **11**, 1807 (1993).
- ²⁷G. Kresse and J. Hafner, *Phys. Rev. B* **47**, 558 (1993).
- ²⁸G. Kresse and J. Furthmuller, *Phys. Rev. B* **54**, 11169 (1996).
- ²⁹G. Kresse and J. Furthmuller, *Comput. Mater. Sci.* **6**, 15 (1996).
- ³⁰G. Kresse, Technische University at Wien, 1993.
- ³¹G. Kresse and J. Hafner, *J. Phys.: Condens. Matter* **6**, 8245 (1994).
- ³²D. Vanderbilt, *Phys. Rev. B* **41**, 7892 (1990).
- ³³V. P. LaBella, H. Yang, D. W. Bullock, P. M. Thiabold, P. Kratzer, and M. Scheffler, *Phys. Rev. Lett.* **83**, 2989 (1999).